Chip-size wavelength detector based on a gradient grating period guided-mode resonance filter

Hsin-An Lin, Hsin-Yun Hsu, and Cheng-Sheng Huang*
Department of Mechanical Engineering, National Chiao Tung University, 1001 Ta Hsueh Rd., Hsinchu, Taiwan 30010

ABSTRACT

In this study, we designed, fabricated and demonstrated a compact wavelength detection system based on a gradient grating period guided-mode resonance filter (GGP-GMRF) mounted on a linear charge-coupled device (CCD) camera. The GGP-GMRF was first fabricated through nanoreplica molding on a plastic substrate, followed by the deposition of a thin TiO_2 film. The grating periods of the GGP-GMRF vary from 250 to 550 nm with a 2 nm increment in each period consisting of 100 cycles. The results show that a 6 mm long GGP-GMRF has a filtering range of 506 to 915 nm. Upon illumination, the GGP-GMRF reflects a particular wavelength of light resulting in the minimum transmission of that wavelength. Hence, the GGP-GMRF provides a spatially dependent minimum transmission depending on the wavelength of the incident light. The linear CCD underneath the GGP-GMRF measures the transmitted intensity, and the wavelength of the incident light can be correlated with the location of the minimum intensity. For the demonstrated GGP-GMRF and CCD system, a spectral resolution of 1 nm can be achieved.

Keywords: linear filter, guided-mode resonance, subwavelength nanostructure

1. INTRODUCTION

Many optical label-free biosensors rely on the detection of the peak wavelength. Through measurement of the peak wavelength shift upon adsorption of biomolecules, the presence or quantity of unknown analytes can be identified. Currently, this is achieved using spectrometers based on diffraction gratings, prisms, or interferometers[1]. Such conventional spectrometers are capable of a high spectral resolution given sufficient distance between the dispersive element and the detection element for wavelength discrimination; however, they are bulky and must be operated off-chip. With the pressing demand for lab-on-a-chip, point-of-care, handheld devices and further integration with smartphones, there is a great need for compact integrated on-chip spectrometers and compact peak wavelength detection systems. Many compact spectrometers have been proposed. Depending on the direction of the dispersed light, they can be broadly classified into in-plane spectrometers, in which incoming light is diffracted into different in-plane directions, and out-of-plane spectrometers, in which scattered light is coupled out of the chip. The mechanisms of these dispersive elements include grating structures, photonic crystals, ring resonators, and Fabry–Perot interferometers[2-8]. Here we propose a new type of dispersive element based on a gradient grating period guided-mode resonance filter (GGP-GMRF).

Wang and Magnusson et al.[16, 17] have shown the GMR phenomenon in a planar dielectric waveguide incorporated with a subwavelength grating structure. The resonance enables external illumination to be coupled into waveguide modes through phase-matching provided by the grating structure. Because of reciprocity, the waveguide modes are immediately coupled out of the waveguide in the specular reflection direction, forming constructive interference with the directly reflected wave. By contrast, the waveguide mode reradiated in the substrate direction destructively interferes with the directly transmitted wave. This phenomenon manifests experimentally as a transmission dip or reflection peak. GMRFs have been demonstrated in one- and two-dimensional grating structures [9-11] with many practical applications[12-15] such as wideband polarizers, label-free biosensors, electro-optic modulators, graded-wavelength GMRFs, optical tunable filters, and fluorescence enhancement.

When a GMRF is illuminated with a broadband light source at normal incidence, a particular wavelength of light excites the resonance of the structure and is reflected, and the rest of the light is transmitted through the filter. The spectral location of the reflection peak or transmission dip corresponds to the resonance wavelength governed by 2nd Bragg condition, which

*csh@nctu.edu.tw; phone 886-3-5712121 55108; fax 886-3-572-0634;

Novel Optical Systems Design and Optimization XIX, edited by Arthur J. Davis, Cornelius F. Hahlweg, Joseph R. Mulley, Proc. of SPIE Vol. 9948, 994809 · © 2016 SPIE
CCC code: 0277-786X/16/$18 · doi: 10.1117/12.2235403

is polarization dependent and highly sensitive to all dimensions of the device. When the grating periods are varied incrementally along the device, a linear wavelength filter can be realized. In this study, we designed, fabricated, and demonstrated a linear variable bandstop filter based on a GGP-GMRF as a dispersive element, such that when the device is incorporated with a photodetector array, a compact wavelength detection system can be realized.

2. GRADIENT GRATING PERIOD GUIDED-MODE RESONANCE FILTER (GGP-GMRF)

2.1 Design and fabrication

In this work, a GMRF was fabricated with gradient grating periods across the device (referred to as a GGP-GMRF), such that it functioned as a linear variable bandstop filter to provide a spatially resolved resonant wavelength. A schematic of the fabricated structure is shown in Fig. 1. The grating period varies from 250 to 550 nm with a 2-nm increment, in which each period consists of 100 cycles. The GGP-GMRF is a three-layer structure consisting of a polyethylene terephthalate (PET) substrate, an UV-curable polymer (NOA68, Norland Products Inc.) with surface relief grating patterns, and a high-refractive-index layer of TiO_2.

The device was fabricated using nanoreplica molding and thin film deposition. In brief, a silicon wafer with gradient grating patterns was fabricated using electron-beam lithography (Leica weprint200) and reactive ion etching. NOA68 (n = 1.556) was sandwiched between the Si master and a sheet of PET. The polymer replica (PET and NOA68) was peeled from the master once the NOA68 had been cured through exposure to ultraviolet light. A layer of TiO_2 (thickness of 134 nm, n = 2.25) was then deposited through sputtering to complete the fabrication for a GGP-GMRF.

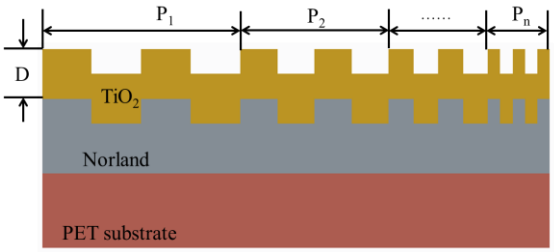

Figure 1. Schematic of the GGP-GMRF.

2.2 Characterization

To verify the accuracy of the fabricated grating structure, scanning electron microscopy was used to characterize the replicated TiO_2/NOA68 grating pattern at the smallest, largest, and moderate periods as shown in Fig. 2. The grating period and duty cycle at 9 periods are summarized in Table 1. For different grating periods, all actual dimensions are within 0.4% of the designed specifications; however, the duty cycles show greater deviations. For the smallest grating periods (250, 252, and 254 nm), the duty cycles are 0.81, 0.79, and 0.80, which are 58.4%–61% greater than the designed specifications. By comparison, for the moderate and large periods, the duty cycles ranged from 0.65 to 0.68, which represent 31.4%–36.4% deviations from the designed duty cycle of 0.5. The deviation on the duty cycle is mainly due to the expansion on the ridge part of the grating after TiO_2 deposition.

Table 1. Summary of the grating periods and duty cycles for different periods.

	Smallest			Moderate			Largest		
Designed Period (nm)	250	252	254	398	400	402	546	548	550
Actual Period (nm)	251	251	255	397	400	403	546	549	552
Deviation (%)	0.4	0.4	0.4	0.3	0	0.2	0	0.2	0.4
Designed Duty Cycle	0.5	0.5	0.5	0.5	0.5	0.5	0.5	0.5	0.5
Actual Duty Cycle	0.81	0.79	0.80	0.66	0.66	0.68	0.65	0.67	0.66
Deviation (%)	61.0	58.4	60.8	31.4	32.4	36.4	30.8	33.6	31.8

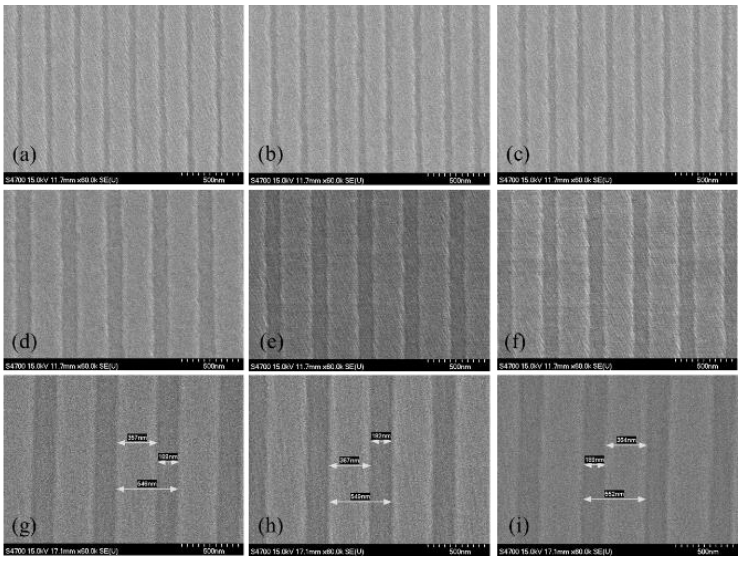

Figure 2. Top view of the gradient GMRF at different locations with periods of (a) 250, (b) 252, (c) 254, (d) 398, (e) 400, (f) 402, (g) 546, (h) 548, and (i) 550 nm.

2.3 Spatial dependent resonance

To demonstrate the spatially dependent resonant wavelength, the GGP-GMRF was mounted on a linear stage with a resolution of 10 µm. A 50 µm optical fiber was connected to a broadband light source (LS-1-LL, Ocean Optics) and was in direct contact with the GMRF. The transmitted light was then collected by another optical fiber connected to a spectrometer (USB2000+VIS-NIR-ES, Ocean Optics). A polarizer was then placed between the transmitted light and the collection fiber to obtain the desired polarization.

The measured transmission spectra with transverse electric (TE) polarization at seven positions from 0 to 6 mm are shown in Fig. 3(a). By gradually moving the translational stage by 1 mm, we measured the transmission spectra at six other locations. The grating periods at the measured locations are approximately 250, 320, 376, 426, 472, 512, and 550 nm. At x = 0 (period = 250 nm), the resonant wavelength is approximately 506 nm, and at x = 6 mm (period = 550 nm), the resonant wavelength is approximately 916 nm. The fabricated gradient GMRF can cover a resonant wavelength of 410 nm.

In addition, we calculated the transmission spectra with TE polarization at the aforementioned periods by using a simulation tool (DiffractMOD, RSoft Design Group) on the basis of a rigorous coupled-wave analysis. The duty cycle and grating depth used in the simulation were 0.68 and 45 nm, respectively. The results (Fig. 3(b)) show that the device exhibits a resonance wavelength of 483 nm (full width at half maximum (FWHM) = 8.24 nm) at a grating period of 250 nm, and a resonant wavelength of 942 nm (FWHM = 12.39 nm) at a grating period of 550 nm. The device can cover an extremely broad spectral range of 459 nm for a grating period range of 300 nm. For both the experimental and calculated results, the resonant wavelengths show linear relationship with the spatial locations of the gradient GMRF as shown in Fig. 3(c).

The major deviation between the simulation and the experimental results is likely due to the following reasons. In the simulation, the absorption and dispersion of the materials including TiO_2, NOA68, and PET were neglected within the wavelength of interest. In addition, the simulation assumed an infinite number of cycles for each grating period; however, for each measurement, the illumination area within a 50 µm optical fiber consisted of only finite numbers of cycles depending on the grating period.

According to the simulation results, when the grating period is greater than 472 nm, the resonant wavelength satisfying the second-order phase-matching conditions begins to appear; hence, two transmission dips can be observed in the transmission spectra. For the grating periods of 472, 512, and 550 nm corresponding to locations of 4, 5, and 6 mm, the second-order phase matching conditions result in transmission dips at 452, 486, and 518 nm, as shown in Fig. 3(b). However, these second-order phase-matching conditions were not observed in the transmission dips in Fig. 3(a). Instead, within the measured wavelength range, the GGP-GMRF exhibits a single resonant wavelength. The deviation between simulation and experimental results is currently under investigation.

The deviation of the measured resonant wavelength from the calculated results is likely due to the dispersion of TiO_2. The TiO_2 refractive index used in the simulation was fixed at 2.25 according to the measurement of the deposited TiO_2 film by using an ellipsometer at 633 nm. Hence, within the resonant wavelength range of 597 nm (at the 1 mm location) to 760 nm (at 3 mm), the experimental and calculated results agree considerably (Fig. 3(c)). The resonant wavelength is proportional to the effective index of the GMRF structure[15]. For both longer and smaller periods with resonant wavelengths distant from 633 nm, because of material dispersion, the deviation between experimental and simulated resonant wavelengths was expected to increase gradually. In practice, at shorter wavelengths (< 633 nm), the refractive index of TiO_2 is expected to be higher than 2.25; hence, the calculated resonant wavelength was underestimated. By contrast, the refractive index decreases with an increase in the operating wavelength, resulting in the measured resonant wavelength being lower than the calculated value. The detailed discussion of the fabrication and characterization can be referred to previous publication[18].

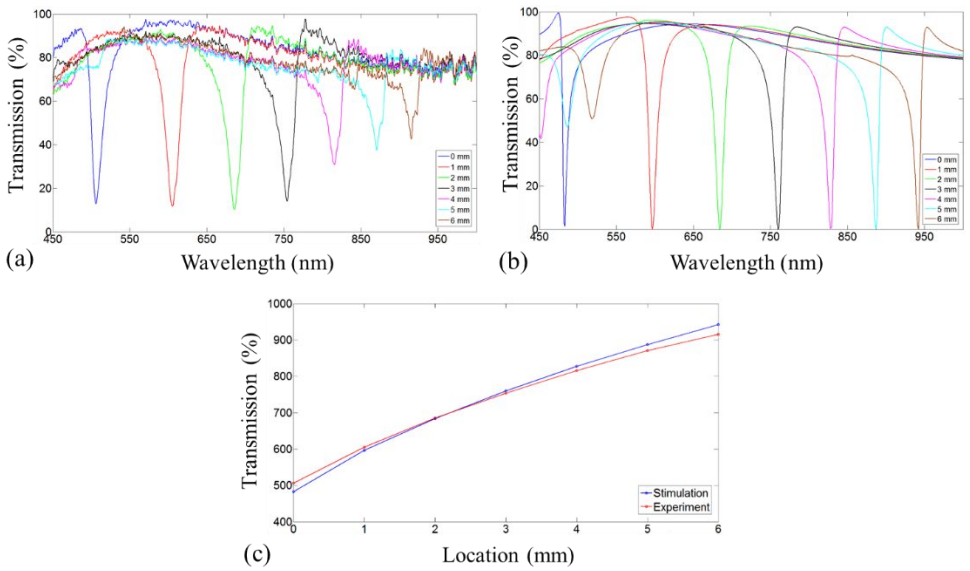

Figure 3. (a) Measured transmission spectra at seven locations. (b) Calculated transmission spectra with grating periods orresponding to the measured locations. (c) Measured and calculated resonant wavelengths at different locations of the fabricated GMRF.

3. WAVELEGNTH DETECTION

The GGP-GMRF was mounted on a 16-bit linear charge-coupled device (CCD) camera with 3648 pixels and a pixel size of 8 × 200 μm. The transverse-electric polarized incident light from a monochromator (DK242, Spectral Products) was expanded to cover the GGP-GMRF. For a specific wavelength of incident light, the resonance at a specific location of the GGP-GMRF is excited. Hence, the light at that location is reflected back and transmitted through the rest of the areas of the GGP-GMRF, enabling the CCD to record the minimum intensity beneath that location. When the wavelength is changed, the light excites the resonance of the GGP-GMRF at another location and the corresponding pixel with the minimum intensity changes accordingly. To demonstrate the wavelength detection capability of the designed GGP-GMRF, the monochromator was used as an illumination source. The incident light was adjusted from 506 to 700 nm in increments of 1.0 nm, and the resulting intensity distribution along the photodetector was recorded. The recorded intensity distribution for four wavelengths, 590, 600, 610, and 620 nm, is shown in Fig. 4. The pixel with the minimum intensity on the CCD is clearly wavelength dependent.

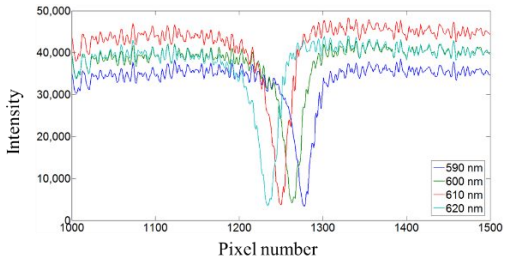

Figure 4. Intensity distribution at the CCD at different incident wavelengths.

As suggested by Ganesh et al.[19] because of the finite bandwidth of the resonance and random electronic noise, the Lorentzian function can be used to fit the intensity profile in the CCD to more accurately define the pixel number corresponding to the minimum intensity. An exemplary Lorentzian fit for the intensity distribution at the photodetector at an incident wavelength of 600 nm is shown in Fig. 5(a), where the pixel number (#1289) corresponding to the minimum intensity can be more accurately found. The relationship between the pixel number corresponding to the minimum intensity and the incident wavelength is shown in Fig. 5(b).

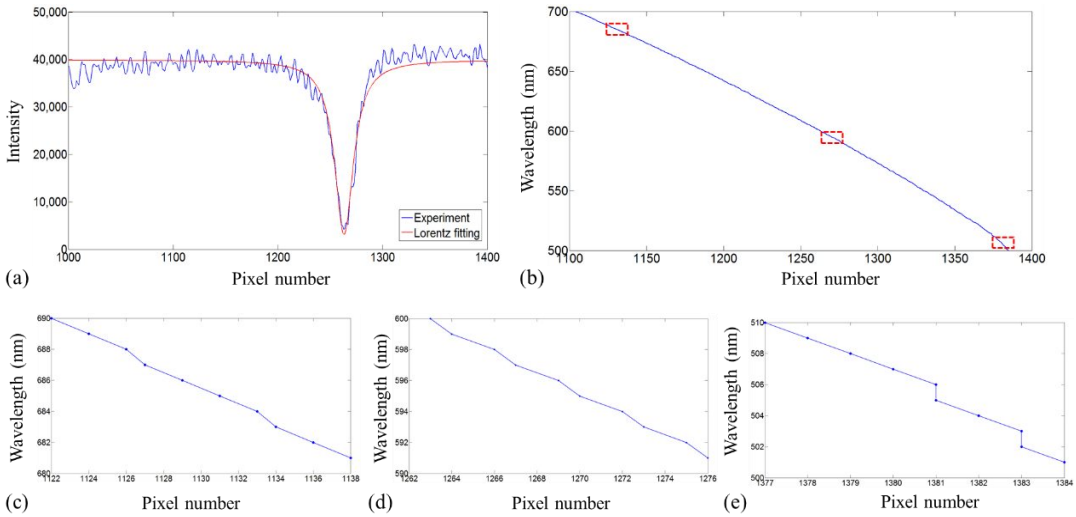

Figure 5. (a) Lorentzian fit of the intensity distribution at an input wavelength of 600 nm. Relationship between the minimum-intensity pixel number and an incident wavelength of (b) 506 to 700 nm, (c) 681 to 690 nm, (d) 591 to 600 nm, and (e) 501 to 510 nm.

The relationship between the incident wavelength and the Lorentzian-corrected minimum-intensity pixel number at three wavelength regions is highlighted in the rectangular boxes of Fig. 5(b). As shown in Fig. 5(c), 5(d), and 5(e), we can clearly resolve 1-nm differences in the incident wavelength in our device, except at 502 and 503 nm, and 506 and 507 nm, for which the pixels are the same. This is probably due to a defect in the Si master fabrication process, which causing these wavelengths resonates at the same location of GGP-GMRF. The resolution is limited by our electron-beam fabrication system. With a higher-resolution fabrication facility, a finer increment on the grating period can be achieved to further improve the spectral resolution.

The slope of the curve indicates the sensitivity of the system, which is not constant. The sensitivity for short, moderate, and long wavelength regions corresponding to the boxes in Fig. 5(b) is 1.29, 0.69, and 0.56 nm/pixel, respectively. In our device, each period consists of 100 cycles. For a period of 250 nm, the total length is 25 μm, which covers approximately 3.125 pixels in the photodetector; by contrast, for a period of 388 nm, the total length is 38.8 μm, which covers approximately 4.85 pixels. For the same amount of variation in incident wavelengths, at longer wavelength regions the resulting minimum-intensity pixel is further separated, as indicated by Fig. 5(c), 5(d), and 5(e).

4. CONCLUSION

In this study, we demonstrated a compact wavelength detection system based on a GGP-GMRF and a linear CCD. The device was fabricated using nanoreplica molding from an e-beam fabricated Si mold and sputtering film deposition on a plastic substrate. The resulting GGP-GMRF consists of gradient grating periods varying from 250 nm to 550 nm (with accuracy within 0.4%) with an increment of 2 nm. By attaching the GGP-GMRF with a linear CCD, the system is able to detect wavelengths from 500 to 700 nm with a 1-nm resolution.

ACKNOWLEDGEMENT

This research was supported by the National Science Council, Taiwan (Grant Nos. NSC 101-2218-E-9-6-MY2 and MOST 103-2221-E-009-075). The authors thank the Nano Facility Center at National Chiao Tung University and National Nano Device Laboratories, Taiwan for their support in the fabrication and characterization of the gradient grating period guided-mode resonance filter.

REFERENCES

[1] Wolffenbuttel, R. F., "MEMS-based optical mini- and microspectrometers for the visible and infrared spectral range," Micromech. Microeng 15(7), S145–S152 (2005).
[2] Xia, Z. X. et al., "High resolution on-chip spectroscopy based on miniaturized microdonut resonators," Opt. Express 19(13), 12356–12364 (2011).
[3] Goldman, D. S., White, P. L., and Anheier, N. C., "Miniaturized spectrometer employing planar wave-guides and grating couplers for chemical-analysis," Appl. Optics 29(31), 4583–4589 (1990).
[4] Sander, D. et al., "Optical microspectrometer in SiON slab waveguides," SPIE 2686, 100–107 (1996).
[5] Momeni, B., Hosseini, E. S., and Adibi, A., "Planar photonic crystal microspectrometers in silicon-nitride for the visible range," Opt. Express 17(19), 17060–17069 (2009).
[6] Pervez, N. K. et al., "Photonic crystal spectrometer," Opt. Express 18(8), 8277–8285 (2010).
[7] Wang, S. W. et al., "Concept of a high-resolution miniature spectrometer using an integrated filter array," Opt. Lett. 32(6), 632–634. (2007).
[8] Wang, S. W. et al., "Integrated optical filter arrays fabricated by using the combinatorial etching technique," Opt. Lett. 31(3), 332–334. (2006).
[9] Winn, J. N., Fink, Y. S., Fan, H., and Joannopoulos, J. D., "Omnidirectional reflection from a one-dimensional photonic crystal," Opt. Lett. 23(20), 1573-1575 (1998).
[10] Boonruang, S., Greenwell, A., and Moharam, M. G., "Multiline two-dimensional guided-mode resonant filters," Appl. Optics 45(22), 5740-5747 (2006).
[11] Peng, S., and Morris, G. M., "Resonant scattering from two-dimensional gratings," Opt. Soc. Am. A. 13(5), 993- 1005 (1996).
[12] Cunningham, B. T., and Laing, L., "Microplate-based, label-free detection of biomolecular interactions: applications in proteomics," Expert Rev. Proteomic 3(3), 271-281 (2006).
[13] Ganesh, N. et al., "Enhanced fluorescence emission from quantum dots on a photonic crystal surface," Nat. Nanotechnol. 2(8), 515-520 (2007)
[14] Dobbs, D. W., Gershkovich, I., and Cunningham, B. T., "Fabrication of a graded-wavelength guided-mode resonance filter photonic crystal," Appl. Phys. Lett. 89(12), 123113-123113-3 (2006).
[15] Magnusson, R. et al., "Leaky-mode resonance photonics: An applications platform," SPIE 8102, 810202-1-810202-13 (2011).
[16] Wang, S. S., and Magnusson, R., "Theory and applications of guided-mode resonance filters," Appl. Optics 32(14), 2606–2613(1993).
[17] Magnusson, R., and Wang, S. S., "New principle for optical filters," Appl. Phys. Lett. 61(9), 1022–1024. (1992).
[18] Lin, H. A., and Huang, C. S., "Linear variable filter based on a gradient grating period guided-mode resonance filter," IEEE Photonics Technol. Lett., 28(9), 1042-1045 (2016)
[19] Ganesh, N. et al., "Compact wavelength detection system incorporating a guided-mode resonance filter," Appl. Phys. Lett., 90(8), 081103-081103-3 (2007).